Organizational Modes of Mesoscale Convective Systems over Central East China

LINLIN ZHENG

Institute of Atmospheric Physics, Chinese Academy of Sciences, and Graduate University of Chinese Academy of Sciences, Beijing, China

JIANHUA SUN

Institute of Atmospheric Physics, Chinese Academy of Sciences, Beijing, China

XIAOLING ZHANG

National Meteorological Center, China Meteorological Administration, Beijing, China

CHANGHAI LIU

National Center for Atmospheric Research, Boulder, Colorado

(Manuscript received 27 August 2012, in final form 12 March 2013)

ABSTRACT

Composite reflectivity Doppler radar data from June to September of 2007–2010 were used to classify mesoscale convective systems (MCSs) over central east China into seven morphologies. The morphologies included one nonlinear mode (NL) and six linear modes: convective lines with no stratiform precipitation (NS), trailing stratiform precipitation (TS), leading stratiform precipitation (LS), parallel stratiform precipitation (PS), bow echoes (BE), and embedded lines (EL). Nonlinear and linear systems composed 44.7% and 55.3% of total MCSs, respectively, but there was no primary linear mode. All MCS morphologies attained their peak occurrence in July, except BE systems, which peaked in June. On average, TS and PS modes had relatively longer lifespans than did other modes.

Significant differences in MCS-produced severe weather existed between dry and moist environments. High winds and hail events were mainly observed in dry environments, and in contrast, short-term intense precipitation occurred more frequently in moist environments. BE systems generated the most severe weather on average, while most TS systems were attendant with short-term intense precipitation and high winds. EL and PS systems were most frequently associated with extreme short-time intense precipitation ($\geq 50\,\mathrm{mm\,h^{-1}}$) as these systems preferentially developed in moist environments. BE systems generally occurred under strong low-level shear and intermediately moist conditions. LS systems were observed in weak low-level shear, whereas EL systems often developed in relatively stable conditions and weak low- to middle-level shear. The largest instability was present in the environment for NS systems. The environmental parameters for TS systems featured the largest differences between the dry and moist cases.

1. Introduction

Severe convective weather, such as intense precipitation, strong wind, and hail, occurred frequently during the warm season over central east China (Tao 1980; Zhang et al. 2008; Xie et al. 2010; Yu et al. 2011). Flash flooding occurred in 1954, 1969, 1980, 1991, 1996, 1998, 1999, 2003, and 2007, and had a significant impact on life and property throughout central east China. For example, the total direct economic losses brought about by the 1954 and 1998 floods are 10,000 million and 166,600 million yuans, respectively (Zong and Chen 2000). The severe wind and hail events occurred suddenly and destroyed buildings and farmland over a short time (Wang et al. 2007; Zheng et al. 2010). Statistical results demonstrated that the direct economic losses brought about by severe convective weather reach up to more than 11 billion

Corresponding author address: Dr. Jianhua Sun, Institute of Atmospheric Physics, Chinese Academy of Sciences, P.O. Box 9804, Beijing 100029, China.
E-mail: sjh@mail.iap.ac.cn

DOI: 10.1175/WAF-D-12-00088.1

yuans every year during 2001–07 (Wang and Cui 2011). Many studies suggested that severe weather events such as wind, hail, and intense precipitation were mostly produced by MCSs (Maddox 1980; Doswell et al. 1996; Schumacher and Johnson 2005; Shibagaki et al. 2000). Numerous mesoscale convective systems (MCSs) are observed to develop and propagate eastward along the frontal zone as the main makers of heavy precipitation in east China (Ding 1993; Bei et al. 2002; Zhao et al. 2004; Sun et al. 2010). For example, the flooding events due to heavy rainfall over the Huaihe basin in 1991 and over the Yangtze River basin in 1998 were produced by MCSs (Ding 1993; Zhao et al. 2004); in particular, the severe heavy rainfall at Wuhan City and Huangshi City, Hubei Province, China, on 20–21 July 1998 resulted from meso-β scale convective systems (MβCSs) (Bei et al. 2002). The study on classifying the morphologies of MCSs had great application in real-time forecasting and warning for MCSs in China.

There have been numerous attempts to classify the morphologies of MCSs using either satellite or radar data. MCS classification was important because different convective organizations may be responsible for producing different types of severe weather, such as heavy precipitation, hail, damaging wind, and tornadoes (Fujita 1978; Gallus et al. 2008, hereafter G2008; Klimowski et al. 2003, hereafter K2003), and may be associated with different dynamical and thermodynamical processes (Bluestein and Jain 1985; Parker and Johnson 2000, hereafter PJ2000; Parker 2007). The pioneering classification study (Maddox 1980) was based on the cold cloud characteristics of infrared satellite images. Mostly according to the horizontal extent, duration, and shape of the $-52°$ and $-32°$C cloud-top temperature thresholds, for instance, Maddox (1980) defined one particular category of MCSs, mesoscale convective complexes (MCCs), in the central United States. Jirak et al. (2003) modified the satellite classification scheme and partitioned several hundred MCSs into four categories: MCCs, persistent elongated convective systems, meso-β-scale circular convective systems, and meso-β-scale elongated convective systems. In China, some studies only investigated the geographic distributions of MCCs using satellite data. Ma et al. (1997) examined the geographical distributions and life cycles of MCSs in China and reported high-frequency occurrences of meso-α-scale convective systems over the middle to lower reaches of the Yellow River and the Yangtze River basins, a result distinct from earlier MCC census studies by Laing and Fritsch (1993, 1997, 2000), where the populations were predominantly from south and southwest China to the South China Sea.

Although their cloud shield features were useful for MCS identification, infrared satellite images could not distinguish the patterns of the underlying convective elements. In contrast, radar imagery provided an effective way of identifying detailed three-dimensional structural information of convective systems, such as the spatial distributions of convective and stratiform development and, consequently, has been increasingly used for MCS classification studies in recent years. On the basis of an 11-yr reflectivity dataset, for example, Bluestein and Jain (1985) documented four distinct formation modes of severe squall lines in Oklahoma during the spring: broken line, back building, broken areal, and embedded areal. This radar-based classification was later extended to nonsevere squall-line development by Bluestein et al. (1987). Blanchard (1990) analyzed basic recurrent features of radar observations in the southern high plains and found three types of mesoscale convective patterns: linear mesoscale systems, occluding mesoscale systems, and chaotic mesoscale systems. According to the arrangement of stratiform precipitation, PJ2000 proposed three morphologies for linear convective systems: those with trailing, leading, and parallel stratiform precipitation. Recently, more complex radar partitioning schemes have been developed primarily in terms of the presence of stratiform precipitation, the arrangement of convective cells and the stratiform region, and the interaction of convective clusters (Jirak et al. 2003; G2008). G2008 collected results from 949 convective storms and radar data occurring in a 10-state region of the central United States during the period 1 April–31 August 2002 and classified the systems into nine morphologies according to the dominant morphology over time exhibited in the radar data. Jirak et al. (2003) studied circular and elongated MCSs on both the large and small scales and classified MCSs into as many as 17 categories during the active convective season of the central United States.

Some studies have attempted to relate severe weather reports to storm morphologies. For instance, it was demonstrated that bow echoes tended to produce more high wind reports (Fujita 1978), and tornadoes were often observed in bow echoes (Trapp et al. 2005) and in supercells (Moller et al. 1994). Pettet and Johnson (2003) showed that leading-stratiform and parallel-stratiform lines produced more flooding events. G2008 analyzed severe weather reports as a function of convective mode and found substantial differences between the types of severe weather reports and the different storm morphologies. Duda and Gallus (2010, hereafter DG2010) indicated that supercellular systems produced severe weather more frequently.

Compared to the significant amount of research into organizational modes of convective systems in North America, very few attempts have been made yet to

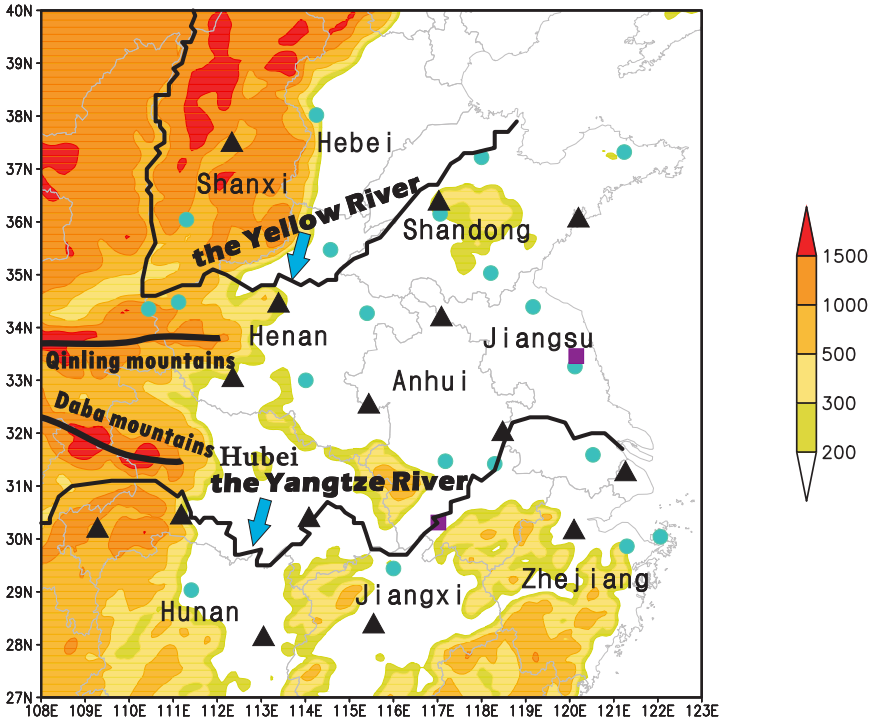

FIG. 1. Distribution of radar and upper-air radiosonde stations over central east China. The purple rectangle represents the radiosonde stations, the green circle represents the radar stations, and the black triangle represents both the radiosonde and radar stations. The shading shows elevations higher than 200 m.

investigate the mesoscale convective morphologies during warm seasons in China. Note that because of the significant influence of the East Asian summer monsoon, considerable differences in large-scale dynamics existed between East Asia and North America. In the summer, the mei-yu front was a unique and primary system affected by the East Asian summer monsoon in east China (Tao 1980). The MCSs during the mei-yu front frequently produced intense precipitation (Ding 1993; Zhao et al. 2004). It has been widely acknowledged that propagating short-wave troughs in the midlatitude jet streams, short-term variations in the southwesterly monsoon flow, changes in the western Pacific subtropical high (WPSH), and the eastward-propagating systems from the Tibetan Plateau are key factors in controlling the mei-yu front precipitation over East Asia (Zhang et al. 2002). In contrast, the convective systems tended to produce strong wind and tornadoes, and the large-scale influencing systems were upper-level jet streams, short-wave troughs in the midlevel, fronts and drylines at the surface over North America (Doswell 1980; Bluestein and Parks 1983; PJ2000). These differences may likely lead to distinct convective organizational characteristics in China. The goal of this study is to document the morphologies of MCSs observed over central east China, analyze their environmental properties, and examine their possible relevance to various severe weather events. The database and methodology are discussed in the following section. In section 3, the morphologies of MCSs identified from multiyear radar observations are classified, and severe weather events attendant with each morphology are analyzed. In addition, severe weather events in dry and moist environments are contrasted. Environmental properties of different linear morphologies are presented in section 4. Finally, a summary and discussion of our findings are given in section 5.

2. Data and methodology

As indicated in Fig. 1, this study focuses on central east China, covering the Yellow River and Huaihe River basins extending southward to the Yangtze River valley, from about 29° to 38°N and 110° to 122°E. The severe storms database was provided by the National Meteorological Center (NMC) of the China Meteorological Administration (CMA), and a total of 47 cases from June to September over a 4-yr period (2007–10) were selected after eliminating those that lacked either radar mosaic or surface observational data (5 cases), those that had bad quality radar data (5 cases), and those that

had not observed the severe weather events (usually severe wind and hail events) because they did not occur in the surrounding area of the weather station (6 cases).

a. Partitioning procedure

In this study, we utilized the national radar mosaic of composite reflectivity provided by the Severe Weather Prediction Center (SWPC) of NMC. The data contained 12 levels of reflectivity factors at 5-dBZ increments (beginning with 10–15 dBZ) with temporal and horizontal resolutions of 10 min and 1 km × 1 km, respectively. The construction of the Doppler radar network in China started in 1998, and as of 2007, there were 112 operational radars. Thirty-five S-band Doppler radar stations and 18 radiosonde stations (Fig. 1) were used to survey the MCS activity over the area of interest. Herein the lifetime of a storm was subjectively determined by the start (end) time of the first (last) radar image where the 30-dBZ contiguous echo coverage exceeded a 30 km × 30 km area with a maximum exceeding 45 dBZ for at least 1 h. The radar echoes meeting the above criteria represented large and persistent convective systems that were well depicted by the composite reflectivity data. Convective and stratiform echoes were defined as those of greater than 40 and 20–40 dBZ, respectively (PJ2000; Geerts 1998). As the pattern of radar echoes varied over the lifetime of a convective system, one individual storm could be classified into different morphologies at its various evolution stages. A radar image sample was attributed to the statistics only when the corresponding morphology persisted for at least 1 h. On the basis of those criteria, a total of 159 morphology samplings were acquired, correspondent to 47 discrete convective cases during the warm seasons of 2007–10. The classification procedure was inherently subjective, as in previous studies (G2008, DG2010).

b. Severe weather events

The severe convective weather reports of different morphological cases were determined by the strongest short-term intense precipitation, the strongest wind, and the largest hail (if available). A morphological case was a stage with morphology unchanged of a storm. Therefore, a morphological case had one intense precipitation, wind, and hail event if observed. The number of intense precipitation (or wind or hail) events divided by the total number of morphologies was the percentage of intense precipitation (or wind or hail) contributed by each morphology. The short-term intense precipitation events were extracted from automatic weather station data, while hail and high-wind events were obtained from significant weather reports. The observational wind was averaged for 2 min. According to the operational rules of SWPC, severe weather reports included short-term intense precipitation with hourly accumulated precipitation > 20 mm, high wind $\geq 17\ \mathrm{m\ s^{-1}}$, and hail ≥ 4 mm in diameter. The events that failed to meet these criteria were recorded as ''weak.'' All severe weather reports were cataloged, including hail ≥ 4 mm but < 10 mm in diameter, hail ≥ 10 mm in diameter, high wind $17 \sim 24\ \mathrm{m\ s^{-1}}$, significant wind $\geq 24\ \mathrm{m\ s^{-1}}$, short-term intense precipitation $\geq 20\ \mathrm{mm\ h^{-1}}$ but $< 50\ \mathrm{mm\ h^{-1}}$, and significant short-term intense precipitation $\geq 50\ \mathrm{mm\ h^{-1}}$. The severe criteria for wind and hail were rather low compared to criteria in the United States (G2008; DG2010). It should be pointed out that high-wind and hail events usually occurred locally and therefore possibly failed to get reported when they did not occur at the observation stations. Also, it is inevitable that bias and quality problems existed at the weather observation data. However, central east China had a relatively uniform density of weather observation stations, which would help to minimize bias and local climatology problems.

c. Physical properties

Physical properties of preconvective environments of the 47 cases were investigated to compare differences between dry and moist MCSs. Additionally, physical properties were investigated to compare differences among linear morphologies. In the calculations of environmental properties of the 47 MCSs cases and 88 linear morphological cases, we selected one single radiosonde observation that best represented the preconvective environment. Because of the coarse spatial and temporal resolutions of the sounding observations, the thermodynamic sounding was reconstructed using a technique similar to that of Johnson and Bresch (1991) and Pan et al. (2008), and the vertical wind profile was reconstructed using the method described by Bluestein and Parks (1983) and Bluestein and Jain (1985). The sounding reconstruction technique involved modifying the 0800 (2000) Beijing time (BJT, BJT = UTC + 8 h) sounding using surface observational data (3-h interval) from noon to afternoon (from midnight to early morning). The sounding from a surface observational station at a required time was reconstructed after modifying the mixing layer of the nearest radiosonde station data, which had the same spatial and temporal resolutions as the surface observational data. To ensure the representativeness of the reconstructed sounding for each case (or morphological case), the radiosonde data were chosen to be within 3 h prior to the formation of the convective system (or morphological case) and 200 km toward the moving direction of the system (or morphological case). However, the radiosonde data were required to be within 250 km and 3 h of the formation of

the convective mode in K2003. Because of the higher density of the spatial resolution of the reconstructed soundings, the criterion of 200 km was enough to ensure the appropriateness of the sounding to a particular case A total of 30 MCSs cases and 61 linear morphological cases were analyzed, excluding events contaminated by precipitation or with poor quality sounding data. A variety of thermodynamic and dynamic quantities as listed in the appendix were diagnosed to characterize environmental conditions of each archetype and to contrast their differences between various categories.

The sounding parameters include the most unstable convective available potential energy (MUCAPE), surfaced-based CAPE (SBCAPE), most unstable convective inhibition (MUCIN), surface-based CIN (SBCIN), downdraft CAPE (DCAPE), the lifted index (LI), and the bulk Richardson number (BRN). Additionally, two kinds of wind shear were calculated, as in K2003. First, the bulk wind shear was determined by taking the vector difference between the surface–500-m mean wind and the wind at a higher level (e.g., 3 or 6 km). Second, the total (also called cumulative) wind shear was obtained by summing the vertical wind shear throughout the depth of the hodograph at 0.5-km intervals, up to the desired level (e.g., 3 or 6 km). As well as the aforementioned quantities, other physical parameters were also calculated for the diagnosis of the convective environment, including the lifting condensation level (PLCL), the most unstable level (PMU), the precipitable water from the surface to 300 hPa (hereafter PWAT), the relative humidity averaged from the surface to 500 hPa (hereafter RH), and the average wind from the surface to 6 km.

3. Morphologies of radar echoes and related severe weather

a. Organizational modes

According to the spatial arrangement of the strongest echoes, the 159 radar imagery (morphology) samplings were first divided into two groups, namely nonlinear (NL) and linear modes. As defined in G2008, NL systems referred to one type of MCSs in which convective cells (≥40 dBZ) were organized in a connected but nonlinear pattern; conversely, linear systems corresponded to another type of MCS in which convective elements (≥40 dBZ) were arranged roughly in a continuous line of at least 75 km in length as well as an eccentricity (major–minor axis) of at least 3 for at least 1 h. The linear group was then subdivided into six categories primarily based on the presence and arrangement of the stratiform region, consisting of convective lines without stratiform rainfall (NS), convective lines with trailing stratiform rainfall (TS), convective lines with leading stratiform rainfall (LS), convective lines with parallel stratiform rainfall (PS), bow echoes (BE), and embedded lines (EL). It should be noted that the TS, LS, and PS morphologies were first proposed by PJ2000 and were later extended to include the NS and BE categories in G2008's linear MCS classification, whereas the last linear morphology, EL, represented a type of MCS that contained a convective line within a large area of weaker, stratiform precipitation, as proposed by Bluestein and Jain (1985). We note the partially qualitative and partially subjective definitions of TS, LS, and PS in PJ2000, but we have not found similar partially qualitative definitions of BE, NS, and EL. Now, we refer to the definitions in PJ2000, and according to the common characteristics of BE, NS, and EL in our study, provide partially qualitative definitions of them.

1) TS

The definitions include a convective line, ''convex toward the leading edge,'' with ''a series of intense reflectivity cells solidly connected by echo of more moderate intensity.'' The line has a very strong reflectivity gradient at (the) leading edge, and a large trailing stratiform precipitation region, often exhibiting a secondary maximum of reflectivity separated from the convective line by a narrow channel of lower reflectivity. BE systems have the same characteristics of trailing stratiform with TS systems. However, some physical characteristics associated with BE systems, such as a rear-inflow jet at the apex, vortices at the ends of the bow (Jorgensen and Smull 1993), downbursts, and microbursts (Fujita 1978), are distinctive of TS systems. In addition, BE systems are often responsible for damaging surface winds and tornadoes (Weisman 2001). Bow-shape displays are see in radar observations of BE systems, but not in TS systems. The criteria without a bow shape are added to the definition of TS systems, which is qualitatively described by the ratio of its arclength to the straight-line distance between the two endpoints of 40-dBZ convective line echoes. The ratio is less than 1.2:1.

2) LS

LS systems were defined to be linear MCSs whose stratiform precipitation is predominantly located in advance of a convective line. In the extreme, members of this class exhibit a convective line preceded by a transition zone and secondary swath of stratiform precipitation with a reflectivity maximum. More frequently, LS MCSs exhibit moderate regions of leading stratiform precipitation without transition zones and secondary bands.

3) BE

Based on the definition of TS in Parker and Johnson (2000), the definition of BE is the same as TS, but with

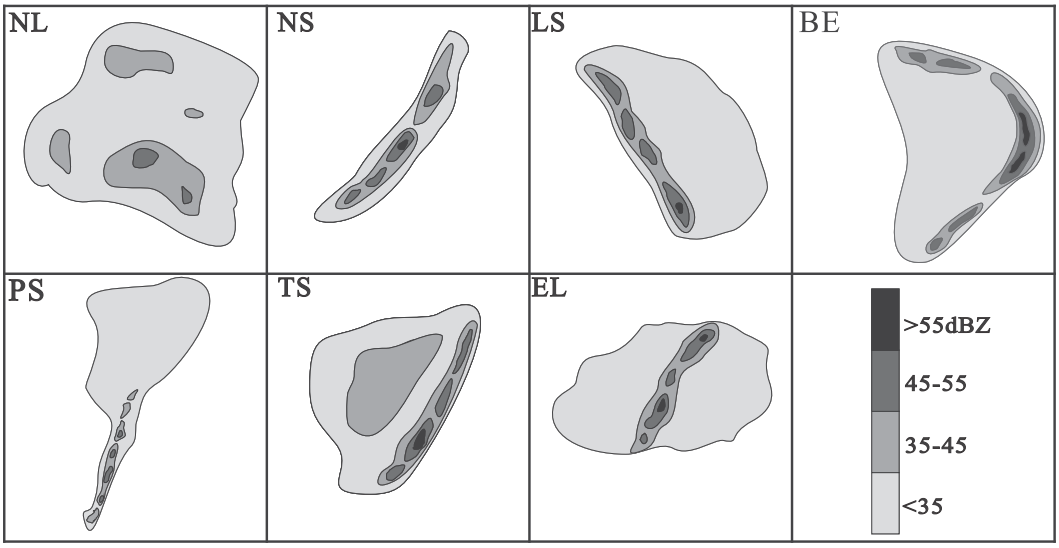

FIG. 2. Schematic reflectivity illustrating each of the seven morphologies in the classification. Morphologies are abbreviated as follow: nonlinear system (NL), squall line with no stratiform rain (NS), squall line with leading stratiform rain (LS), bow echo (BE), squall line with parallel stratiform rain (PS), squall line with trailing stratiform rain (TS), and embedded line (EL). The NL, NS, LS, BE, PS, and TS morphologies are adapted from G2008.

a bow of the line. A bow echo must appear as a crescent-shaped echo (40 dBZ roughly in a continuous line) in radar reflectivity data. The crescent-shaped echo is qualitatively described by the ratio of its arclength to the straight-line distance between the two endpoints of 40-dBZ convective line echoes. The ratio is larger than/or equal to 1.2:1.

4) NS

An NS features a series of intense reflectivity cells solidly connected by echoes of more moderate intensity. The line has a very strong reflectivity gradient at (the) leading and trailing edges. The maximum width of each side stratiform precipitation region is less than that of the line.

5) EL

The line echoes are embedded in stratiform precipitation. The reflectivity gradient is relatively large on both sides of the convective line and the maximum width of the preline and postline stratiform precipitation is larger than that of the line.

6) PS

To distinguish between PS and EL systems, the definition of a PS system is modified. The northern part of the line echoes are embedded in stratiform precipitation, with at least 1/3 of the line echoes (southern part) having a very strong reflectivity gradient at the leading and trailing edges. Most or all of the stratiform precipitation region associated with the convective line moves parallel to the line itself (within a storm-relative framework) and to the left of the line's motion vector throughout its life cycle. The stratiform regions' movements in PS cases generally deviate less than 30° from the convective lines' orientation.

A schematic illustrating the basic organizational fashions of these seven morphologies is shown in Fig. 2. Although BE systems with a ''bow'' or ''crescent shape'' in the radar reflectivity could also be classified as TS systems as indicated in G2008, we preferentially separated BE from TS because BE systems were found to be closely related to high-wind and hail events over the study region.

The radar observations in Fig. 3 exemplify the six linearly organized categories. The squall line on 26 August 2009 was a typical NS system, which extended ~1000 km along the northeast–southwest orientation and had no apparent stratiform precipitation. In contrast, the southeastward-moving 20 June 2008 case was a well-developed LS system, characteristic of a large stratiform area being 3–4 times as wide as the convective area behind. Although both cases contained significant trailing stratiform precipitation, the BE system on 14 June 2008 had much stronger convective echoes than did the TS system on 29 June 2007. In the PS system on 1 July 2008, stratiform precipitation was mainly observed at the northern end of the system. The 5 June 2009 case corresponded to a quasi-stationary EL system with stratiform precipitation straddling both sides of the convective line.

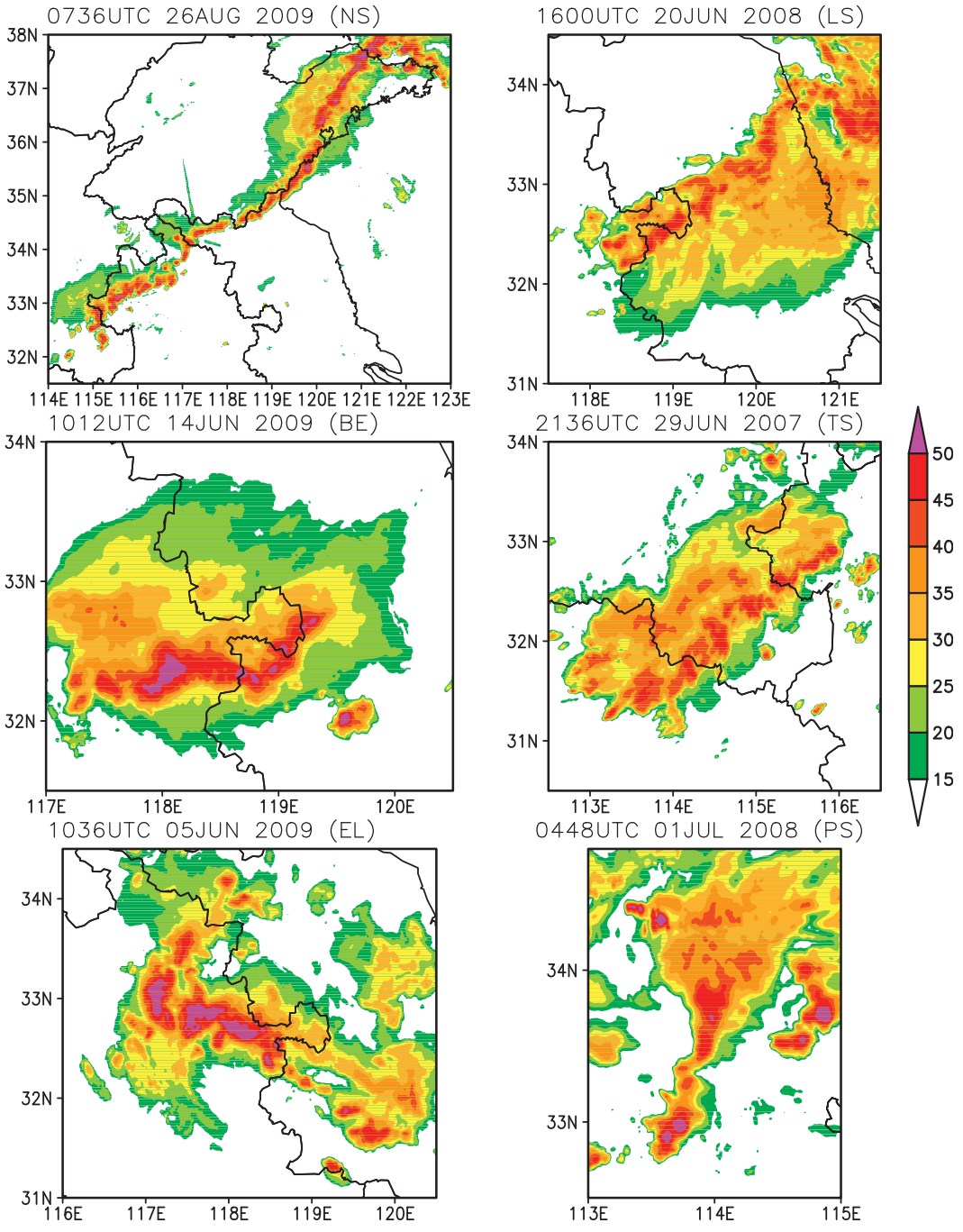

FIG. 3. Radar images for the (top left) observed NS system on 26 Aug 2009, (top right) the LS system on 20 Jun 2008, (middle left) the BE system on 14 Jun 2009, (middle right) the TS system on 29 Jun 2007, (bottom left) the EL system on 5 Jun 2009, and (bottom right) the PS system on 1 Jul 2008.

b. Distributions and transitions of organizational modes

Figure 4 presents the percentage distribution of each morphology among the total morphological population and the percentage of each linear mode among the linear morphological population only. Nonlinear systems (71) were common, accounting for 44.7% of the total (159) cases, and all types of linear systems (88) together composed the remaining 55.3%. The large proportion of linear organization herein was more than twice as much as the counterpart for the central United States reported

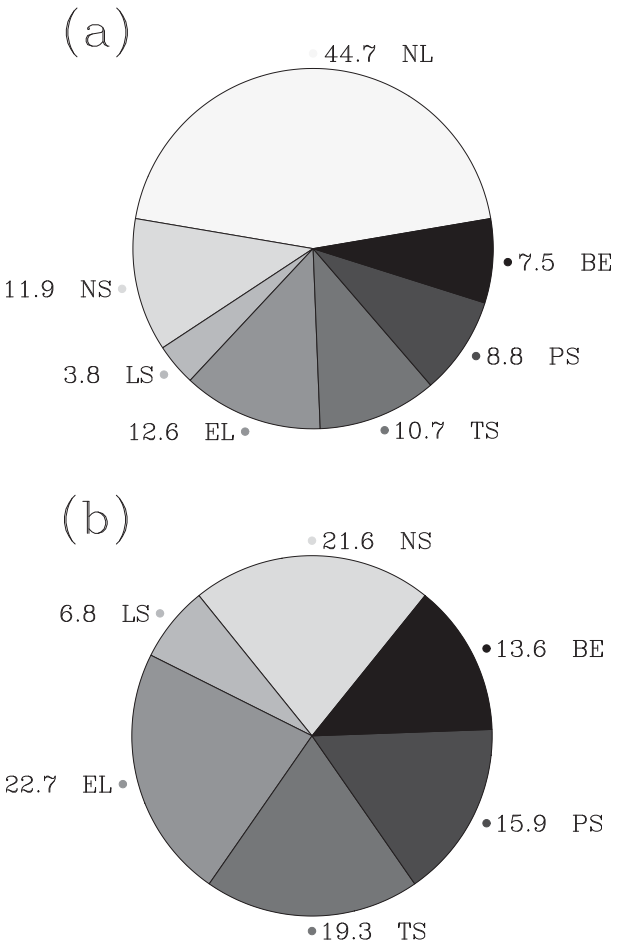

FIG. 4. Percentage distribution of (a) each morphology among the 159 morphological samples and (b) each linear morphology among the 88 linear morphological samples.

by G2008. This geographical contrast, however, could arise partially from the different classification techniques used; the working sample in G2008 consisted of separate convective events that were partitioned according to the dominant morphology during the life cycle of storms, whereas the current statistics were based on the morphological samplings of radar images. LS systems contributed very little to the whole population, similar to G2008 and DG2010, but their rare occurrence here may be a result of the small sample size. The other linear systems (i.e., NS, EL, TS, PS, and BE) showed comparable proportions, ranging from 7.5% to 12.6%.

Of the 88 linear cases, EL morphology was the most prevalent with a proportion of 22.7% (Fig. 4b). The relatively high occurrence compared to that over North America (Bluestein and Jain 1985) was consistent with the fact that most of the summertime convective systems over central east China were associated with large-scale stratiform precipitation along the mei-yu front (Ding 1993; Ninomiya 2000; Zhao et al. 2004). NS (21.6%) and TS (19.3%) morphologies were ranked the second and third most frequent, respectively, with the least occurrence for BE (13.6%) and PS (15.9) systems. A striking difference from G2008 and PJ2000 was the absence of a primary linear organizational mode over central east China.

Of the 47 cases, the initial modes were dominated by NL (23 cases) and NS (13 cases) systems (Fig. 5), which represents 76.7% of all cases. Only 23.3% of linear systems begin in one of the other five modes. NL and NS systems are dominant initially and they have the first and third highest frequency of occurrence among the systems (Fig. 4), which may indicate that the environmental conditions of NL and NS are preferential to reveal in the future study. Two-thirds (66.7%) of BE systems occurred in the intermediate morphologies of MCSs, and 50% of PS systems occurred in the final morphologies (Fig. 5).

c. Geographical distribution and duration

The initial (genesis) time of a convective system was defined to be the time when the strongest composite reflectivity first reached 45 dBZ and the 30-dBZ reflectivity covered at least 30 km $\times$ 30 km. The location was the centroid point of the strongest echo or the geometric center if the strongest echoes were scattered. The spatial distribution of the genesis location of the 47 MCSs displayed two concentrated areas (Fig. 6a): one was centered over Henan and Hubei Provinces, which are located to the east of high mountains (Qinling and Daba Mountains; see Fig. 1), and the other was over northern Anhui Province, which is located along the Huaihe River basin. About 80% of the documented MCS cases initiated around these two areas, revealing that the distribution of terrain is an important factor for triggering convection possibly through regional-scale mountain–plains solenoids, which can be induced by differential heating between the high mountain ranges in central east China and the low-lying plains in eastern China (Sun and Zhang 2012).

The initial locations of nonlinear and linear morphologies are shown in Figs. 6b and 6c, respectively. The genesis of the nonlinear systems (Fig. 6b), albeit more scattered, was similar to that of the MCS samplings (Fig. 6a). They mostly initiated over central eastern Henan, northwestern Anhui, and central western Jiangsu Province. The genesis of the linear archetypes, especially for PS, EL, and BE systems, was concentrated near the junction of Henan and northern Anhui Provinces, as well as at the central junction of Anhui and Jiangsu (Fig. 6c). TS and NS systems were relatively scattered. The sources of linear archetypes (Fig. 6c) were mostly located east of

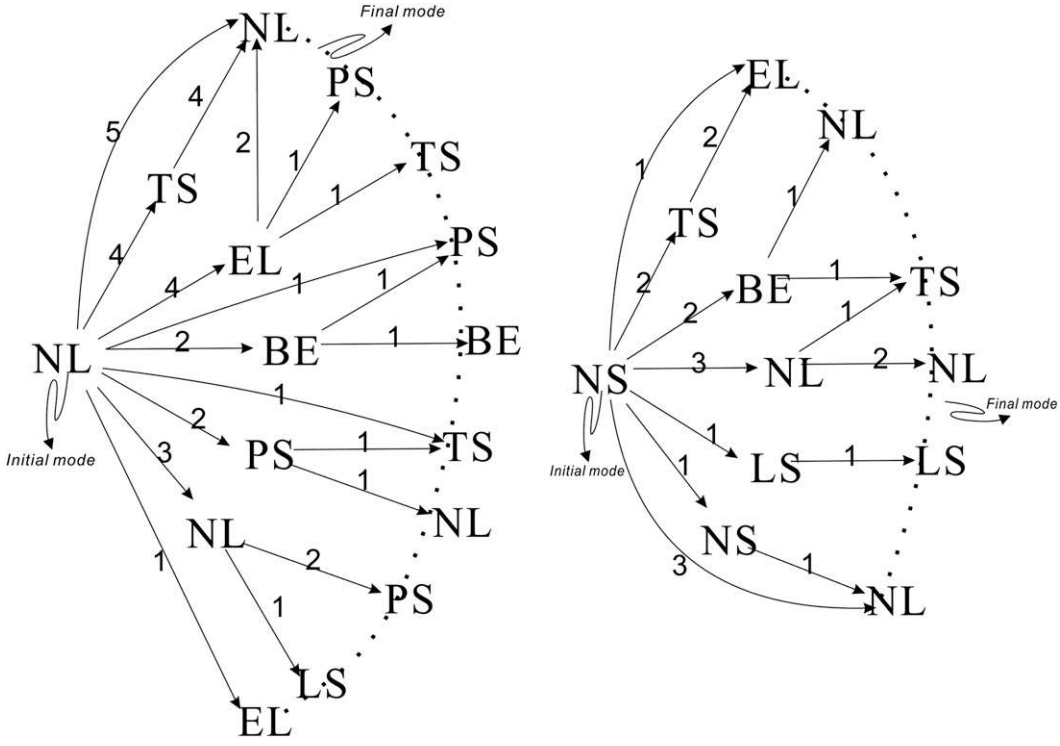

FIG. 5. Illustration of evolutionary pathways for MCSs. Labels along each pathway denote the initial, dominant morphology in intermediate stage, and the final modes. The total number of cases following each step is indicated.

the sources of MCSs (Fig. 6a), which could be a consequence of eastward-propagating convection from the high mountains (Qinling and Daba Mountains) (He and Zhang 2010; Bao et al. 2011).

As shown in Fig. 7a, 73.4% of MCSs had a lifetime of more than 9 h. The average lifetime of MCSs was 14 h. The average lifetime of MCSs over China was longer than that over North America (Geerts 1998; PJ2000). More than half of the morphological population lasted for less than 3 h, and approximately a quarter of NL systems and one-third of linear systems survived for 3–6 h (Figs. 7b and 7c). Accordingly, nearly 85% of the systems had a duration of 1–6 h (Table 1), and only a small fraction of NL (12.7%) and linear (15.9%) systems could persist for longer than 6 h. Of the six linear modes, TS (4.5 h) and PS (5 h) systems were relatively more persistent than NS (4 h), LS (3.8 h), EL (3.9 h), and BE (4 h) systems. Additionally, the lifetime of NL (3.85 h) systems was somewhat shorter than most linear systems except the LS type.

d. Monthly and diurnal distribution

The majority of the morphologies peaked in July, except for bow echoes, which showed a June maximum (Fig. 8a). The lowest occurrence occurred in September for all morphologies. The frequent observation of the BE category in the early summer was likely related to the relatively strong shear and intense interactions between the northern cold-dry air with southern warm-moist air over central east China during this time of the year (Liang and Sun 2012).

The diurnal variations of deep convection and precipitation over east China differed substantially from region to region and were determined by many factors, such as synoptic circulation and terrain distribution (Xu and Zipser 2011; Bao et al. 2011; Sun and Zhang 2012). Although MCSs could be triggered at any time of the day, the genesis pattern displayed a clear maximum at 1300–2000 BJT and a secondary maximum at 0000–0400 BJT (Fig. 8b), consistent with the double-peak pattern in diurnal cycles of thunderstorms documented in this region (Zheng et al. 2011), while the diurnal variation was apparently different from the late evening peak in the U.S. MCS cases (Wallace 1975; PJ2000).

e. Severe weather reports

The relationship between MCS morphology and severe weather reports is investigated here. Figure 9 presents the percentage of morphologies associated with a given type of severe weather report. Intense precipitation was the most common severe weather, reaching 65% for all archetypes and over 80% for TS, EL, and BE systems. This

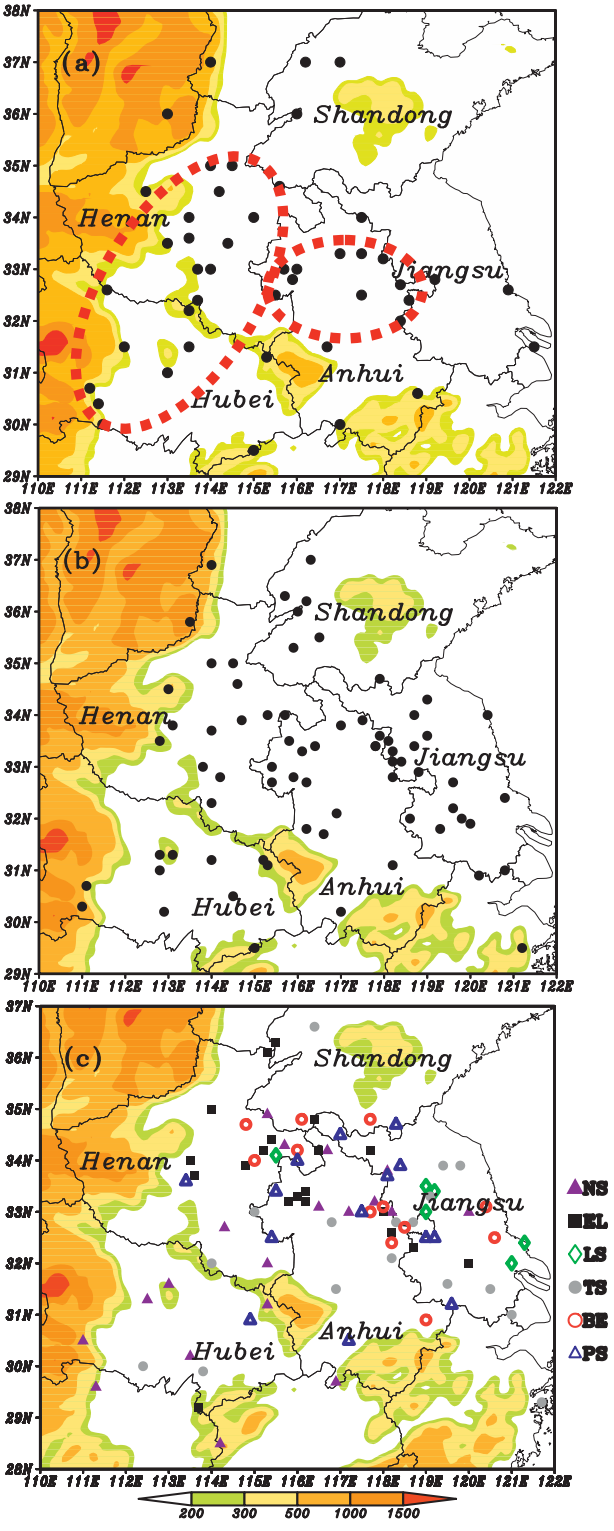

FIG. 6. Geographical distribution of initial locations for (a) the 47 discrete MCS cases, (b) NL systems, and (c) linear systems (NS, EL, LS, TS, BE, and PS). The shading shows elevations higher than 200 m.

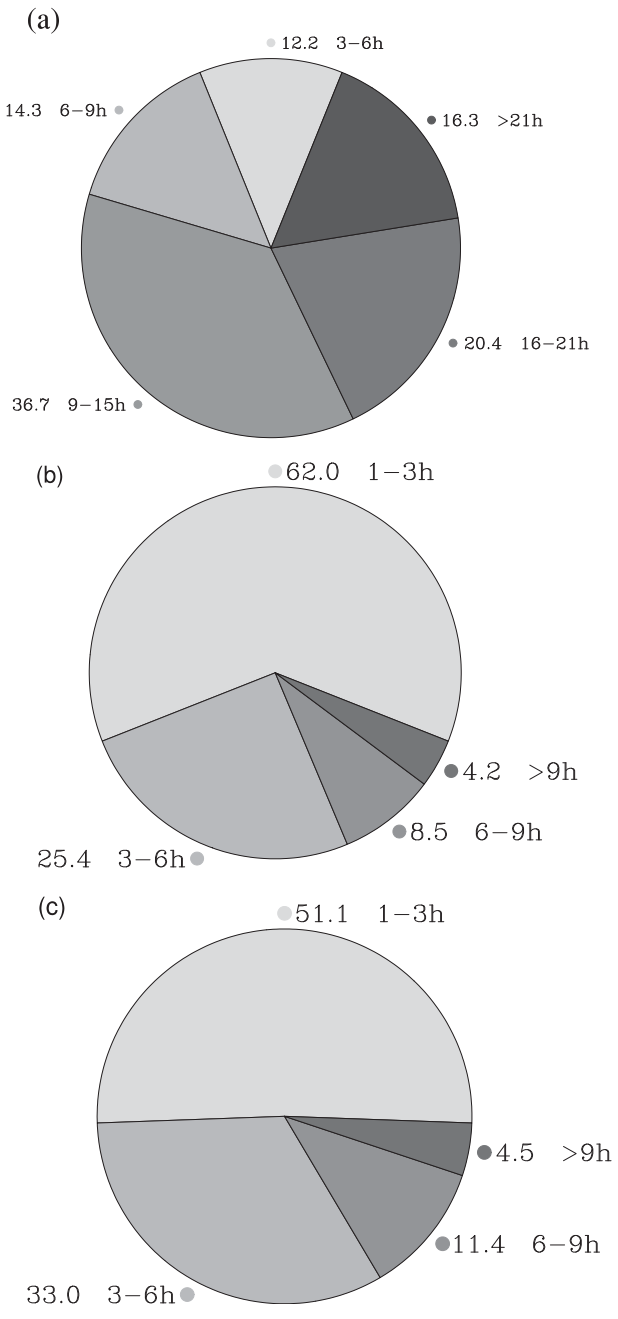

FIG. 7. Percentage distribution as a function of longevity for (a) all MCSs, (b) nonlinear systems, and (c) linear systems.

was in contrast with the results of Parker (2007), G2008, and DG2010, where it was found that PS systems produced the greatest number of flash floods per system. For high-wind events the BE category (50%) was most prolific, as indicated by G2008 and DG2010, followed by TS (41.2%) and LS (33.3%) systems. NS and BE systems were the leading producers of hail events, although hail events were the least common among the three types of

TABLE 1. Lifetime (h) of each morphology.

Morphology No.	NL	Linear systems					
		NS	LS	EL	TS	BE	PS
1–3	44	10	4	13	8	6	4
3–6	18	8	2	4	5	4	6
6–9	6	1	0	3	3	2	1
>9	3	0	0	0	1	0	3
Avg lifetime	3.9	4.0	3.8	3.9	4.5	4.0	5.0

severe weather. Additionally, none of the hail events was associated with LS and PS systems. G2008 and DG2010 reported that broken line (BL) systems were the most conducive for hail events in the central United States. Their result was in broad agreement with the present study, considering that BL systems are classified as NS systems herein.

We further analyzed the possible correspondence between each morphology and the following particular weather type: rain only (R), high wind only (W), rain and high wind (RW), hail and rain (HR), high wind and hail (WH), and rain, high wind, and hail (RWH) (Fig. 10). It is readily seen that R was most common for all morphologies. TS systems generated RWs comparable to R events. Additionally, hail events always accompanied either rain or wind or even both. Another interesting point was that EL and PS systems only generated events associated with intense precipitation. This may suggest that EL and PS systems tended to develop in moist environmental conditions (see later).

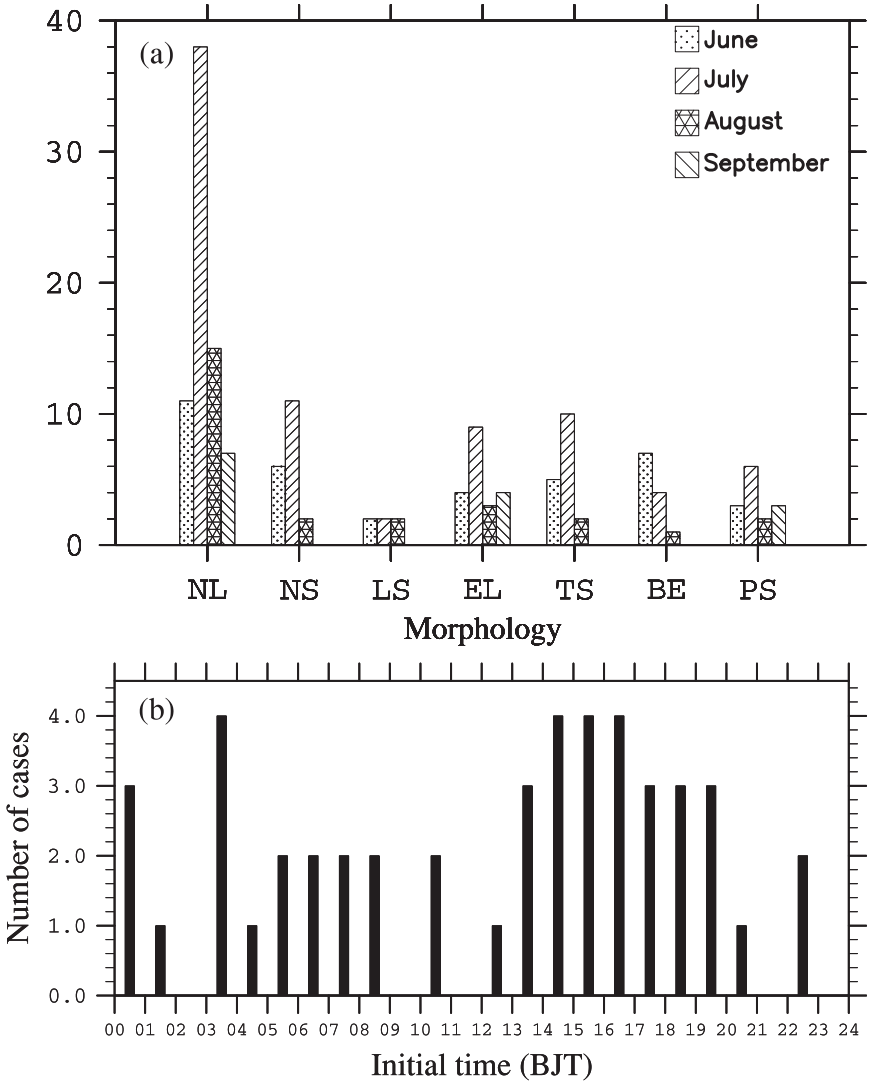

FIG. 8. (a) Number of each morphology as a function of month, and (b) diurnal distribution of genesis time for the 47 discrete MCS cases. Times are BJT, where BJT = UTC + 8 h.

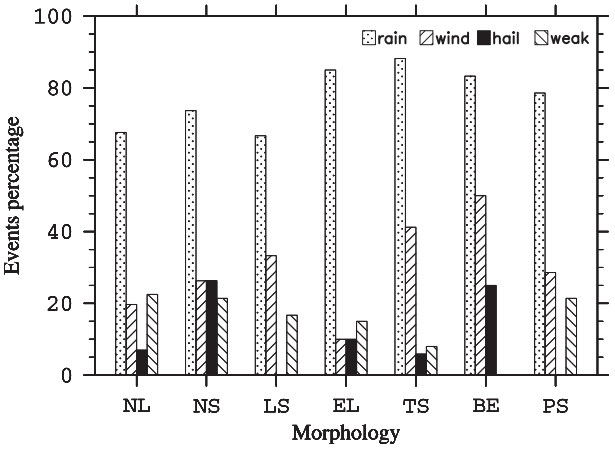

FIG. 9. The percentage of morphologies associated with a given type of severe weather report.

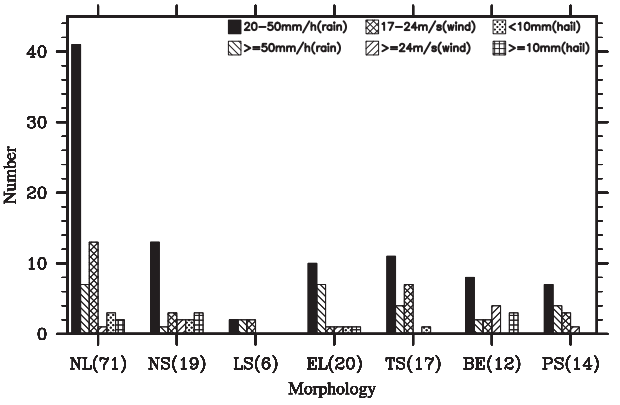

FIG. 11. As in Fig. 10, but for different weather types: intense rainfall (20–50 mm h^{-1}), extremely intense rainfall (≥50 mm h^{-1}), high winds (17–24 m s^{-1}), extremely high winds (≥24 m s^{-1}), hail (<10 mm), and large hail (≥10 mm).

The three types of severe weather were each divided into two subranges to facilitate the comparisons between different morphologies. Short-term intense precipitation (20–50 mm h^{-1}) was most common for most archetypes (Fig. 11). EL systems were most effective in producing significant short-term intense precipitation (≥50 mm h^{-1}). TS systems led the production of high winds (17–24 m s^{-1}), while BE systems were the top morphology type for extremely high winds (≥24 m s^{-1}). All hail events associated with BE systems fell into the large-hail range (≥10 mm in diameter), but most of the hail events of 4 ~ 10 mm in diameter were observed in NS systems. These results differed substantially from the findings of G2008, who found that PS systems were connected with more significant hail reports, but none of the hail events occurred with these systems in the present study (Figs. 9 and 10). In general, the linear systems were more prone to generating severe weather (79.3% intense precipitation, 31.6% high wind, and 11.2% hail) than the NL systems (67.6% intense precipitation, 19.7% high wind and 7.0% hail), as evinced in Fig. 12. As mentioned above, the severe criteria for wind and hail were rather lower compared to the criteria in the United States (hail ≥ 25.4 mm and wind ≥ 26 m s^{-1}). Only 5/47 cases (7/159 morphological cases) and 2/47 cases (2/159 morphological cases) were observed for wind ≥ 26 m s^{-1} and hail ≥ 25.4 mm, respectively.

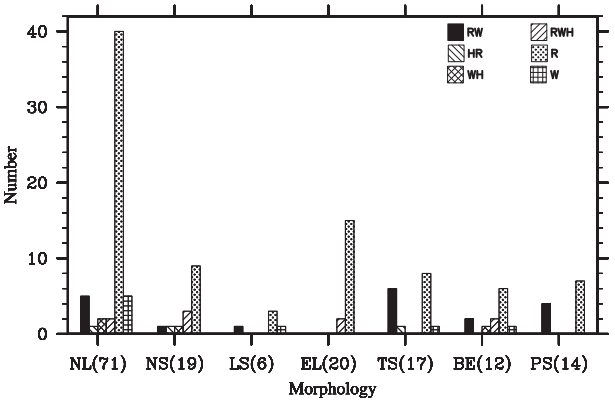

FIG. 10. Number of severe weather types associated with each morphology. Types are abbreviated as follow: rain only (R); high wind only (W); rain and wind event (RW); hail and rain event (HR); wind and hail event (WH); and rain, wind, and hail event (RWH). The values in parentheses represent the number of each morphology.

f. Contrast between dry and moist environments

The East Asian summer monsoon brings warm and moist air from the Indian and western Pacific Oceans to eastern China (Tao 1980), making the MCSs over

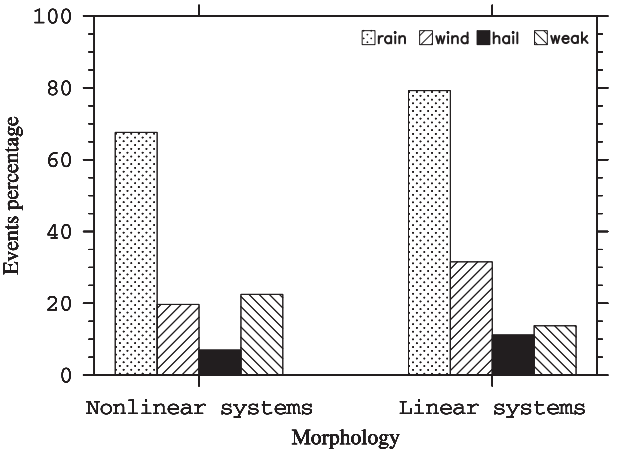

FIG. 12. As in Fig. 9, but for nonlinear and linear systems.

central east China very productive for rainfall (Ding 1993; Zhao et al. 2004). Nevertheless, not all MCSs therein were observed in moist environments. Some of these events were triggered in relatively dry environments before the moist summer monsoonal airflow reached central east China in the early summer. We calculated the precipitable water (PWAT) from the surface to 300 hPa in the 47 MCS cases using the 6-hourly National Centers for Environmental Prediction (NCEP) Final Analysis (FNL) dataset because radiosonde data for some events were not available. The results showed that the short-term intense precipitation events tended to be associated well with PWAT greater than 50 mm (herein defined as a moist environment), whereas the environment with PWAT less than 50 mm (herein defined as a dry environment) was favorable for the generation of high-wind and hail events. The numbers of dry and moist cases were 10 (21.3%) and 37 (78.7%), respectively. The threshold of PWAT was 22–34 mm in Bluestein and Jain (1985). In the study, eight dry cases had PWAT of 15–35 mm, and the other two cases had PWAT of 40–50 mm, which produce strong wind events. These may demonstrate that 50 mm was the best discriminator in a statistical sense. Most dry cases (8 of 10) were observed in June when the East Asian summer monsoon had not yet advanced to central east China.

Of the 159 morphological populations, 27 cases (17%) were observed in dry environments, and the remaining 132 cases (83%) developed in moist environments. The weather events were also divided into two groups according to the environments of their associated morphologies. As indicated in Fig. 13a, short-term intense precipitation in moist environments (78.8%) was more frequent than that in dry environments (55.6%), but high winds in dry environments were 4 times as much as those in moist environments. Additionally, all hail events were observed in dry environments. As shown in Fig. 13b, dry environments were prone to RWH events, reaching up to 33.3%. In contrast, R and RW weather events were relatively more prolific in moist environments.

Although only a minor difference between dry and moist environments existed in the frequency of short-term precipitation with an intensity of 20–50 mm, significant short-term intense precipitation ($\geq$50 mm h^{-1}) events mostly occurred in moist conditions (Fig. 13c). The severe wind (17–24 m s^{-1}) was more than twice as common in dry environments as in moist environments, and in particular, a majority of significant high-wind events (eight out of nine cases) were associated with dry environments. Hail and significant winds rarely occurred in moist environments.

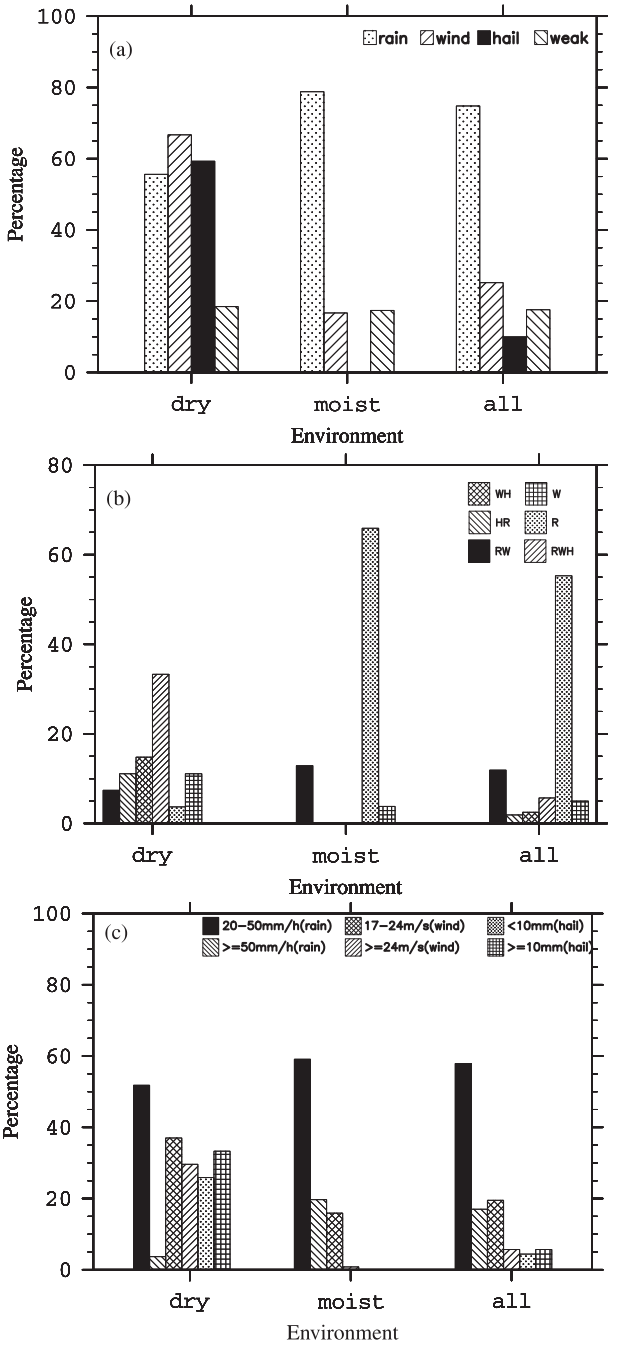

FIG. 13. Percentage distribution of various weather types produced by all morphological populations in dry, moist environments and all environments. (a) Four weather types: rain events (hourly rainfall > 20 mm), wind events ($\geq$17 m s^{-1}), hail events ($\geq$4 mm), and weak events. (b) Six weather types: rain only (R), high wind only (W), rain and high wind (RW), hail and rain (HR), high wind and hail (WH), and rain, high wind and hail (RWH). (c) Six weather types: intense rainfall (20–50 mm h^{-1}), extremely intense rainfall ($\geq$50 mm h^{-1}), high winds (17–24 m s^{-1}), extremely high winds ($\geq$24 m s^{-1}), hail (<10 mm), and large hail ($\geq$10 mm).

TABLE 2. Average values and standard deviations (in parentheses) of thermodynamic and dynamic parameters in preconvective environments of all, dry, and moist MCS cases.

Parameter	All	Dry	Moist
PLCL (hPa)	919 (69)	842 (63)	952 (39)
PMU (hPa)	986 (38)	1002 (4)	979 (44)
MUCAPE ($J\,kg^{-1}$)	2344 (1360)	3094 (1097)	2023 (1356)
MUCIN ($J\,kg^{-1}$)	13 (26)	26 (43)	7 (13)
SBCAPE ($J\,kg^{-1}$)	2188 (1447)	3091 (1099)	1801 (1421)
SBCIN ($J\,kg^{-1}$)	23 (39)	21 (43)	24 (39)
DCAPE ($J\,kg^{-1}$)	661 (470)	1119 (418)	464 (341)
LI (K)	−4.95 (3.17)	−8.67 (1.46)	−3.36 (2.19)
Surface–300-hPa PWAT (mm)	52.4 (16.0)	32.0 (11.6)	61.5 (7.1)
Surface–500-hPa average RH (%)	68.7 (19.42)	42.7 (10.93)	80.3 (8.0)
0–3-km bulk shear ($m\,s^{-1}$)	10.38 (4.12)	8.15 (3.35)	11.39 (4.10)
0–3-km total shear ($m\,s^{-1}$)	16.30 (4.55)	15.36 (5.43)	16.73 (4.17)
0–6-km bulk shear ($m\,s^{-1}$)	14.06 (3.98)	12.21 (4.58)	14.90 (3.49)
0–6-km total shear ($m\,s^{-1}$)	24.21 (5.77)	22.83 (6.97)	24.83 (5.22)
0–6-km avg wind ($m\,s^{-1}$)	8.28 (3.87)	6.83 (3.32)	8.94 (4.00)
Bulk Richardson No.	79.28 (95.92)	162.84 (126.50)	45.86 (55.35)

4. Environmental characteristics of linear modes

a. Contrast between dry and moist cases

Since the weather types strongly depended on the environmental moisture conditions as demonstrated above, physical properties of preconvective environments of the 10 ''dry'' cases and the 37 ''moist'' cases were compared in detail. Based on the technique described in section 2, 9 dry cases and 21 moist cases were analyzed, excluding events contaminated by precipitation or with sounding data of poor quality. All PWAT calculations using radiosonde data were very similar to the results using the NCEP FNL dataset.

As illustrated in Table 2, most parameters varied markedly between the dry and moist conditions. The large standard deviation for some parameters, such as MUCAPE, SBCAPE, SBCIN, and MUCIN, was indicative of a considerable overlap among these parameters of different morphologies. The large standard deviation for radiosonde parameters also existed in the previous studies (Bluestein and Jain 1985; K2003). On the whole, the average PWAT (32 mm) in dry environments was comparable to the results of the past studies, for example, 28 mm for convection lines (Bluestein and Jain 1985) and 26.9 mm for severe convective windstorms (K2003), as well as 33.5 mm for TS systems, 32.7 mm for LS systems, and 24.3 mm for PS systems (PJ2000), as shown in Table 3. It seems that while convection occurred, however, the corresponding SBCAPE ($3091\,J\,kg^{-1}$) and LI were greater than for the North American cases (PJ2000; Bluestein and Jain 1985; K2003), which indicated that the accumulated energy was stronger in dry

TABLE 3. Comparison of physical properties derived from the environmental soundings of MCSs between different studies. A dash (—) indicates the corresponding parameter is unavailable.

Domain	Sounding parameters		SBCAPE ($J\,kg^{-1}$)	SBCIN ($J\,kg^{-1}$)	LI (K)	LCL (hPa)	PWAT (mm)	BRN
Central east China	Present study	All events	2188	23	−4.95	919	52.4	79.28
		Dry	3091	21	−8.67	842	32.0	162.84
		Moist	1801	24	−3.36	952	61.5	45.86
		Line echoes	1820	34	−4.26	915	54.1	51.5
East China	Meng and Zhang (2012)	Pre-TC squall lines	1548	67	−3.6	899	61.0	—
East China	Meng et al. (2013)	Squall lines	1568	61	−4.0	916	59.3	—
OK	Bluestein and Jain (1985)	All lines	2260	33	—	—	28.0	64
Central United States	PJ2000	LS	1009	—	−3.5	811	32.7	—
		PS	813	—	−2.2	765	24.3	—
		TS	1605	—	−5.4	831	33.5	—
Northern U.S. high plains	K2003	Windstorms	1974	−71	—	—	26.9	58

TABLE 4. Average physical parameters as a function of linear mode in dry and moist environments. Values in parentheses represent the numbers of sounding samples and all samples, respectively.

	BE (8/12)		TS (12/17)		PS (10/14)		LS (5/6)		NS (17/19)		EL (9/20)	
Parameter Environment	Dry (4/4)	Moist (4/8)	Dry (3/3)	Moist (9/14)	Dry (0/2)	Moist (10/12)	Dry (0/0)	Moist (5/6)	Dry (5/5)	Moist (12/14)	Dry (3/3)	Moist (6/17)
PLCL (hPa)	842	922	910	955		949		943	861	935	851	950
PMU (hPa)	957	968	1001	1000		994		1002	1002	992	996	973
MUCAPE ($J\,kg^{-1}$)	2097	1926	1192	2554		1877		2151	2372	2557	1891	1491
MUCIN ($J\,kg^{-1}$)	23	28	151	17		6		6	32	4	18	32
SBCAPE ($J\,kg^{-1}$)	1534	1440	1192	2177		1663		1921	2366	2331	1891	1419
SBCIN ($J\,kg^{-1}$)	31	55	151	33		19		18	23	26	18	46
DCAPE ($J\,kg^{-1}$)	745	708	1542	685		346		493	1283	424	957	710
LI (K)	−5.30	−3.28	−4.41	−4.19		−3.55		−4.12	−6.76	−4.22	−6.55	−3.30
PWAT(mm)	35.1	58.3	23.7	62.2		62.8		59.5	25.3	65.4	30.0	59.3
RH (%)	54	73	27.46	74.08		80.99		77.45	36.02	80.03	52.67	75.89
0–3-km bulk shear ($m\,s^{-1}$)	11.08	12.46	12.43	10.38		11.38		9.02	10.50	10.20	7.95	10.34
0–3-km total shear ($m\,s^{-1}$)	23.86	18.30	18.57	16.19		19.97		15.41	18.70	16.92	15.24	16.15
0–6-km bulk shear ($m\,s^{-1}$)	13.09	11.92	16.55	14.46		15.44		15.13	14.45	14.38	18.71	11.62
0–6 km total shear ($m\,s^{-1}$)	31.45	27.04	27.71	24.73		28.74		24.01	27.93	24.06	27.18	22.21
0–6-km avg wind ($m\,s^{-1}$)	9.96	13.02	9.44	8.93		10.56		10.5	9.12	10.43	9.79	7.61
BRN	94	38	38	53		27		48	93	53	55	58

environments over central east China. The high PWAT (61.5 mm) in moist cases bore a strong resemblance to the results of pre–tropical cyclone (TC) squall lines that occurred over southern China (Meng and Zhang 2012; Meng et al. 2013). The LI, LCL, and PWAT results of line echoes are generally consistent with those of squall lines in east China (Meng et al. 2013).

The instability parameters, such as PLCL (842 hPa), SBCAPE ($3091\,J\,kg^{-1}$), MUCAPE ($3094\,J\,kg^{-1}$), and DCAPE ($1119\,J\,kg^{-1}$), in dry cases were larger than those in moist cases (PLCL, 952 hPa; SBCAPE, $1801\,J\,kg^{-1}$; MUCAPE, $2023\,J\,kg^{-1}$; and DCAPE, $464\,J\,kg^{-1}$). The lower LI in dry cases implied weaker stratification than in moist cases. The higher MUCIN in dry cases needed stronger a triggering factor for the development of MCS than in moist cases. The bulk shear, total shear, and average wind were stronger in moist cases, while the weak shear and stratification in dry cases resulted in a considerably higher BRN, which, in fact, was the highest among all studies listed in Table 3. Strong low- to middle-level shear and wind in moist cases may indicate the frequent presence of a low-level jet (LLJ) that aided in the transport of moisture into central east China prior to the triggering of MCSs, consistent with some case studies (Zhang et al. 2010; Sun et al. 2010). Higher CAPE and DCAPE in dry environments could explain why these MCSs produced higher winds and more hail than in moist environments.

b. Physical description of linear morphologies

Table 4 compared moisture, thermodynamic, and wind shear parameters for each linear morphology in dry and moist environments. Linear systems (except the TS category) in dry environments had larger SBCAPE and smaller SBCIN values than those in moist environments, as well as higher PLCL, lower LI, and larger shear. These differences implied that the development of linear systems in dry conditions required relatively stronger instability and wind shear. Note that the values of shear parameters were larger in moist cases than in dry cases in Table 2, which was inconsistent with the results in Table 4. This contradiction was because these quantities in Table 2 were calculated in the preconvective stage of convective systems, whereas most of them were calculated in the intermediate morphologies of convective systems in Table 4 (most linear morphologies developed in the intermediate morphologies of convective systems). The inconsistency led to a hypothesis that the low- to middle-level shear played different roles in the initial and intermediate morphologies of MCSs, an issue warranting further study in the future.

The BE systems in dry environments displayed the second largest MUCAPE ($2097\,J\,kg^{-1}$), and the highest BRN (94), PWAT (35.1 mm), and RH (54%) (Table 4). These results were consistent with those of K2003, where it was found that PWAT and RH for bow echoes were higher than other types of storms. However, BE systems in moist environments had the lowest PWAT (58.3 mm) and RH (73%) among all morphologies. Therefore, it is tempting to conclude that BE systems could be triggered under strong low- to middle-level wind shear and CAPE in an intermediate moist background (i.e., the "moist" dry environments or "dry" moist environments).

The instability parameters (SBCAPE, MUCAPE, SBCIN, and MUCIN) and moisture parameters for the TS systems featured the largest differences between the dry and moist cases (Table 4). The moist cases were characteristic of much higher MUCAPE and SBCAPE but smaller MUCIN and SBCIN than the dry cases. As most of the NS systems were observed in the early stages of MCSs, it can be deduced that the MCS initiation required a strong instability. They shared many commonalities with the BE morphology in dry environments and with the TS morphology in moist environments.

The PS systems in moist environments corresponded to the low PLCL (949 hPa), SBCIN (19 J kg^{-1}), MUCIN (6 J kg^{-1}), and DCAPE (346 J kg^{-1}), but the large PWAT (62.8 mm) and RH (80.99%) (Table 4). The very moist conditions herein were in stark contrast with the results of PJ2000, where it was noticed that the average PWAT of PS systems was only 24.3 mm and smaller than in TS and LS systems. This geographical differentiation may suggest that the mechanisms driving the PS systems affected by the East Asian summer monsoon differ from those in North America. The abundant moisture associated with the PS systems was conducive to intense precipitation, especially extreme rainfall events (Fig. 11). Additionally, the smallest BRN appeared in the PS systems.

As most of the EL systems occurred in moist environments, they had the smallest MUCAPE (1491 J kg^{-1}), SBCAPE (1419 J kg^{-1}), and 0–6-km average wind (8.43 m s^{-1}) (Table 4). On the other hand, they had relatively larger MUCAPE values (1819 J kg^{-1}) and the smallest MUCIN (18 J kg^{-1}) in dry environments among all of the morphologies. Although the EL systems in moist environments produced a high frequency of intense precipitation, some of them produced high winds and hail under low PWAT (~30 mm, the second smallest in dry environments).

5. Summary and conclusions

A total of 47 severe convective cases (159 morphological cases) were detected from June to September 2007–10 in central east China. The MCSs identified from radar images were first cataloged into seven morphologies, including one nonlinear mode and six linear modes. Then, the severe weather reports and the environmental characteristics associated with each organizational mode were investigated. In addition, the preconvective characteristics were compared between dry and moist environments in view of the apparent distinction of the associated severe weather. Finally, the environmental properties for six linear modes were analyzed.

Nonlinear and linear systems composed 44.7% and 55.3%, respectively, of the total samples. EL systems occurred most frequently among the six linear modes. Their genesis was concentrated within two areas: to the east of a mountainous region (Qinling and Daba Mountains), and the Huaihe River basin. The activity of MCSs peaked in July, except for in the BE category, which peaked in June.

Intense precipitation exhibited the highest frequency in each morphology, especially in EL and TS systems. BE systems had the highest probability of high winds and hail, especially significant wind ($\geq$24 m s^{-1}) and large hail ($\geq$10 mm in diameter). The R events had the highest frequency, with EL systems being the principal producer. TS and PS systems were most prone to RW events. Hail was found to be always accompanied by other types of weather. The significant short-term intense precipitation ($\geq$50 mm h^{-1}) was often associated with the EL and PS systems. High winds ($\geq$17 but <24 m s^{-1}) were most frequently present in TS systems. In summary, BE systems were more likely to produce high winds and hail. Consistent with DG2010, BE systems were considered the "dangerous" morphology since they produce the largest proportion of damaging severe weather by a morphological case and no weak weather associated with it.

Most short-term intense precipitation, especially extremely intense precipitation, occurred in moist environments, whereas high winds were mainly observed in dry environments and hail was not observed in moist environments. The dry environments were characteristic of higher PLCL, CAPE, DCAPE, CIN, and BRN, but lower LI and vertical shear than in moist environments. The greater SBCAPE and LI observed in dry cases indicated stronger accumulated energy in dry environments over central east China. The MCSs in moist environments will be studied and compared with the MCSs in dry environments in the future.

The environmental properties associated with BE systems displayed the largest low-level shear, 0–6-km average wind, BRN, PWAT, and RH in dry environments and the smallest PWAT and RH in moist environments. It was noted that too dry or too moist conditions are unfavorable for the development of BE systems. The parameters for TS systems featured the largest differences between the dry and the moist environments. The corresponding parameters of the NS systems were similar to those for BE systems in dry environments and those for TS systems in moist environments. The environmental properties of PS and EL systems and their associated weather were quite different from those in the central United States. Their structure and organization mechanisms will be further studied by real-case analyses and simulations.

Because of the limitations of radar data and surface observational data, only 47 discrete MCS cases were

documented. In the future, a larger sample size of MCSs will be investigated to allow us to draw more robust conclusions.

Acknowledgments. We thank Arlene Laing and John Tuttle for reviews of the draft manuscript and comments. The station data and Doppler radar data were provided by the National Meteorological Center, China Meteorological Administration. This research was supported by the National Natural Science Foundation of China under Grants 41075032 and 40930951, the China Meteorological Administration under Grant GYHY200906004, and the National Key Basic Research and Development Project of China under Grant 2012CB417201.

APPENDIX

Sounding Indices

a. MUCAPE and SBCAPE

The most unstable CAPE is

$$\mathrm{MUCAPE} = g\int_{Z_{\mathrm{LMU}}}^{Z_{\mathrm{EL}}} \frac{T_{vp} - T_{ve}}{T_{ve}}\,dz$$

and surface-based CAPE is

$$\mathrm{SBCAPE} = g\int_{Z_S}^{Z_{\mathrm{EL}}} \frac{T_{vp} - T_{ve}}{T_{ve}}\,dz,$$

where Z_{LMU} is the most unstable level with the maximum equivalent potential temperature; Z_S is the height of the surface level; T_{vp} and T_{ve} are the virtual temperatures of the environment and an air parcel, respectively; Z_{LFC} is the level of free convection; and Z_{EL} is the equilibrium level.

b. MUCIN and SBCIN

The most unstable CIN is

$$\mathrm{MUCIN} = g\int_{Z_{\mathrm{LFC}}}^{Z_{\mathrm{LMU}}} \frac{T_{vp} - T_{ve}}{T_{ve}}\,dz$$

and the surface-based CIN is

$$\mathrm{SBCIN} = g\int_{Z_{\mathrm{LFC}}}^{Z_s} \frac{T_{vp} - T_{ve}}{T_{ve}}\,dz.$$

c. DCAPE

The downdraft convective available potential energy is

$$\mathrm{DCAPE} = g\int_{Z_s}^{Z_D} \frac{T_{ve} - T_{vp}}{T_{ve}}\,dz,$$

where Z_D is the height of the downdraft-starting level.

d. LI

The lifted index is

$$\mathrm{LI} = T_{500} - T_{\mathrm{p500}},$$

where T_{500} is the environmental temperature at 500 hPa and T_{p500} is the temperature of an air parcel lifted adiabatically from the surface to 500 hPa.

e. BRN

The bulk Richardson number is

$$\mathrm{BRN} = \frac{\mathrm{CAPE}}{\frac{1}{2}U^2},$$

where U is the magnitude of the vector difference between the 0–6-km mean wind and the 0–500-m mean wind.

REFERENCES

Bao, X., F. Zhang, and J. Sun, 2011: Diurnal variations of warm-season precipitation east of the Tibetan Plateau over China. *Mon. Wea. Rev.,* **139,** 2790–2810.

Bei, N. F., S. X. Zhao, and S. T. Gao, 2002: Numerical simulation of a heavy rainfall event in China during July 1998. *Meteor. Atmos. Phys.,* **80,** 153–164.

Blanchard, D. O., 1990: Mesoscale convective patterns of the southern high plains. *Bull. Amer. Meteor. Soc.,* **71,** 994–1005.

Bluestein, H. B., and C. Parks, 1983: A synoptic and photographic climatology of low-precipitation severe thunderstorms in the southern plains. *Mon. Wea. Rev.,* **111,** 2034–2046.

——, and M. H. Jain, 1985: Formation of mesoscale lines of precipitation: Severe squall lines in Oklahoma during the spring. *J. Atmos. Sci.,* **42,** 1711–1732.

——, G. T. Marx, and M. H. Jain, 1987: Formation of mesoscale lines of precipitation: Nonsevere squall lines in Oklahoma during the spring. *Mon. Wea. Rev.,* **115,** 2719–2727.

Ding, Y. H., 1993: *Study on the Lasting Heavy Rainfalls over the Yangtze–Huaihe River Basin in 1991* (in Chinese). Chinese Meteorological Press, 255 pp.

Doswell, C. A., III, 1980: Synoptic-scale environments associated with high plains severe thunderstorms. *Bull. Amer. Meteor. Soc.,* **61,** 1388–1400.

——, H. E. Brooks, and R. A. Maddox, 1996: Flash flood forecasting: An ingredients-based methodology. *Wea. Forecasting,* **11,** 560–581.

Duda, J. D., and W. A. Gallus Jr., 2010: Spring and summer midwestern severe weather reports in supercells compared to other morphologies. *Wea. Forecasting,* **25,** 190–206.

Fujita, T. T., 1978: Manual of downburst identification for Project Nimrod. Satellite and Mesometeorology Research Paper 156,

Dept. of Geophysical Sciences, University of Chicago, 104 pp. [NTIS PB-286048.]

Gallus, W. A., Jr., N. A. Snook, and E. V. Johnson, 2008: Spring and summer severe weather reports over the Midwest as a function of convective mode: A preliminary study. *Wea. Forecasting,* **23,** 101–113.

Geerts, B., 1998: Mesoscale convective systems in the southeast United States during 1994–95: A survey. *Wea. Forecasting,* **13,** 860–869.

He, H., and F. Zhang, 2010: Diurnal variations of warm-season precipitation over north China. *Mon. Wea. Rev.,* **138,** 1017–1025.

Jirak, I. L., W. R. Cotton, and R. L. Mcanelly, 2003: Satellite and radar survey of mesoscale convective system development. *Mon. Wea. Rev.,* **131,** 2428–2448.

Johnson, R., and J. Bresch, 1991: Diagnosed characteristics of precipitation systems over Taiwan during the May–June 1987 TAMEX. *Mon. Wea. Rev.,* **119,** 2540–2557.

Jorgensen, D. P., and B. F. Smull, 1993: Mesovortex circulations seen by airborne Doppler radar within a bow-echo mesoscale convective system. *Bull. Amer. Meteor. Soc.,* **74,** 2146–2157.

Klimowski, B. A., M. J. Bunkers, M. R. Hjelmfelt, and J. N. Covert, 2003: Severe convective windstorms over the northern high plains of the United States. *Wea. Forecasting,* **18,** 502–519.

Laing, A. G., and J. M. Fritsch, 1993: Mesoscale convective complexes over the Indian monsoon region. *J. Climate,* **6,** 911–919.

——, and ——, 1997: The global population of mesoscale convective complexes. *Quart. J. Roy. Meteor. Soc.,* **123,** 389–405.

——, and ——, 2000: The large-scale environments of the global populations of mesoscale convective complexes. *Mon. Wea. Rev.,* **128,** 2756–2776.

Liang, J. Y., and J. H. Sun, 2012: The formation mechanism of damaging surface wind during the squall line in June 2009 (in Chinese). *Chin. J. Atmos. Sci.,* **36,** 316–336.

Ma, Y., X. Wang, and Z. Tao, 1997: Geographic distribution and life cycle of mesoscale convective system in China and its vicinity (in Chinese). *Prog. Nat. Sci.,* **7,** 583–589.

Maddox, R. A., 1980: Mesoscale convective complexes. *Bull. Amer. Meteor. Soc.,* **61,** 1374–1381.

Meng, Z., and Y. Zhang, 2012: On the squall lines preceding landfalling tropical cyclones in China. *Mon. Wea. Rev.,* **140,** 445–470.

——, D. Yan, and Y. Zhang, 2013: General features of squall lines in east China. *Mon. Wea. Rev.,* **141,** 1629–1647.

Moller, A. R., C. A. Doswell III, M. P. Foster, and G. R. Woodall, 1994: The operational recognition of supercell thunderstorm environments and storm structures. *Wea. Forecasting,* **9,** 327–347.

Ninomiya, K., 2000: Large- and meso-α-scale characteristics of meiyu–baiu front associated with intense rainfalls in 1–10 July 1991. *J. Meteor. Soc. Japan,* **78,** 141–157.

Pan, Y. J., K. Zhao, and Y. N. Pan, 2008: Single-Doppler radar observation of a heavy precipitation supercell on a severe squall line (in Chinese). *Acta Meteor. Sin.,* **66,** 621–636.

Parker, M. D., 2007: Simulated convective lines with parallel stratiform precipitation. Part I: An archetype for convective in along-line shear. *J. Atmos. Sci.,* **64,** 267–288.

——, and R. H. Johnson, 2000: Organizational modes of midlatitude mesoscale convective systems. *Mon. Wea. Rev.,* **128,** 3413–3436.

Pettet, C. R., and R. H. Johnson, 2003: Airflow and precipitation structure of two leading stratiform mesoscale convective systems determined from operational datasets. *Wea. Forecasting,* **18,** 685–699.

Schumacher, R. S., and R. H. Johnson, 2005: Organization and environmental properties of extreme-rain-producing mesoscale convective systems. *Mon. Wea. Rev.,* **133,** 961–976.

Shibagaki, Y., M. D. Yabanaka, S. Shimizu, H. Uyeda, A. Watanabe, Y. Maekawa, and S. Fukao, 2000: Meso-β- to meso-γ-scale wind circulations associated with precipitating clouds near baiu front observed by the MU and meteorological radars. *J. Meteor. Soc. Japan,* **78,** 69–91.

Sun, J., and F. Zhang, 2012: Impacts of mountain–plains solenoid on diurnal variations of rainfalls along the mei-yu front over the east China plains. *Mon. Wea. Rev.,* **140,** 379–397.

——, S. X. Zhao, G. K. Xu, and Q. T. Meng, 2010: Study on a mesoscale convective vortex causing heavy rainfall during the meiyu season in 2003. *Adv. Atmos. Sci.,* **27,** 1193–1209.

Tao, S. Y., 1980: *Heavy Rainfalls in China* (in Chinese). Science Press, 225 pp.

Trapp, R. J., S. A. Tessendorf, E. S. Godfrey, and H. E. Brooks, 2005: Tornadoes from squall lines and bow echoes. Part I: Climatological distribution. *Wea. Forecasting,* **20,** 23–34.

Wallace, J. M., 1975: Diurnal variations in precipitation and thunderstorm frequency over the conterminous United States. *Mon. Wea. Rev.,* **103,** 406–419.

Wang, X., and C. Cui, 2011: A number advances of the research on the heavy rain mesoscale convective systems (in Chinese). *Torrential Rain and Disasters,* **30,** 97–106.

——, W. Mao, and J. Guo, 2007: Statistical features of strong convective weather disaster in China in 2004 main flood period (in Chinese). *J. Nat. Disasters,* **16,** 27–30.

Weisman, M. L., 2001: Bow echoes: A tribute to T. T. Fujita. *Bull. Amer. Meteor. Soc.,* **82,** 97–116.

Xie, B., Q. Zhang, and Y. Wang, 2010: Observed characteristics of hail size in four regions in China during 1980–2005. *J. Climate,* **23,** 4973–4982.

Xu, W. X., and E. J. Zipser, 2011: Diurnal variations of precipitation, deep convection, and lightning over and east of the eastern Tibetan Plateau. *J. Climate,* **24,** 448–465.

Yu, R., X. Zhang, G. Li, and Q. Gao, 2011: Analysis of frequency variation of thunderstorm, hail and gale wind in eastern China from 1971 to 2000 (in Chinese). *Meteor. Monogr.,* **38,** 1207–1216.

Zhang, C., Q. Zhang, and Y. Wang, 2008: Climatology of hail in China: 1961–2005. *J. Appl. Meteor. Climatol.,* **47,** 795–804.

Zhang, S. L., S. Y. Tao, and Q. Y. Zhang, 2002: Large and mesoscale characteristics of intense rainfall in the mid and lower reaches of the Yangtze River. *Chin. Sci. Bull.,* **47,** 779–786.

Zhang, X., S. Tao, and J. Sun, 2010: Ingredients-based heavy rainfall forecasting (in Chinese). *Chin. J. Atmos. Sci.,* **34,** 754–766.

Zhao, S. X., Z. Y. Tao, J. H. Sun, and N. F. Bei, 2004: *Study on Mechanism of Formation and Development of Heavy Rainfalls on Mei-Yu Front in Yangtze River* (in Chinese). China Meteorological Press, 282 pp.

Zheng, L. L., J. H. Sun, and J. Wei, 2011: The diurnal variation of thunder events in China (in Chinese). *Torrential Rain Disasters,* **30,** 137–144.

Zheng, Y., X. Zhang, Q. Zhou, Y. Duan, Y. Chen, and L. He, 2010: Review on convective weather short-term forecasting and nowcasting (in Chinese). *Meteor. Monogr.,* **36** (7), 33–42.

Zong, Y., and X. Chen, 2000: The 1998 flood on the Yangtze, China. *Nat. Hazards,* **22,** 165–184.